1 From discontinuous models towards a continuum description

Marc Lätzel, Stefan Luding, and Hans J. Herrmann

Institute for Computer Applications, University of Stuttgart, Pfaffenwaldring 27, 70569 Stuttgart, Germany

Abstract. One of the essential questions of material sciences is how to bridge the gap between microscopic quantities, like contact forces and deformations, in a granular assembly, and macroscopic quantities like stress, strain or the velocity-gradient. A two-dimensional shear-cell is examined by means of discrete element simulations. Applying a volume averaging formalism, one obtains volume fractions, coordination numbers, and fabric properties. Furthermore, the stress tensor and the "elastic" (reversible) mean displacement gradient can be derived. From these macroscopic quantities, some material properties can be computed by different combinations of the tensorial invariants.

Because an essential ingredient of both simulations and experiments are rotations of the independent grains, we apply a Cosserat type description. Therefore we compute quantities like the couple stress and the curvature tensor as well as a combination of them, the "torque-resistance".

1.1 Introduction

Macroscopic continuum equations for the description of the behavior of granular media rely on constitutive equations for stress, strain, and other physical quantities describing the state of the system. One possible way to obtain an observable like, for example, the stress is to perform discrete particle simulations [1–3] and to average over the "microscopic" quantities in the simulation, in order to obtain the averaged macroscopic quantity. Besides the trivial definitions for averages over scalar and vectorial quantities like density, velocity, and particle-spin, one can find slightly different definitions for stress and strain averaging procedures in the literature [3–12] (see also the contributions by Cambou, Goddard, Kruyt and Lanier in this book).

The aim of this paper is to review recent results for tensorial, averaged continuum quantities, and to present new results connected to the rotational degrees of freedom. In section 1.2 the setup of the system is described and the simulation method is discussed. In section 1.3 our averaging method is introduced and in section 1.4 applied to some scalar quantities. Section 1.5 contains the definitions and averaging strategies for fabric, stress, and elastic deformation gradient and, in addition, some material properties are extracted from their combinations. The rotations of our particles are taken into account in section 1.6 and averages are presented for the corresponding macroscopic quantities.

1.2 Model System and Simulation

1.2.1 The Couette Shear-cell Setup

In the simulations presented in this study, a two-dimensional Couette shear-cell is used, as sketched in Fig. 1.1. N particles are confined between an outer ring and an inner ring with radius R_o and R_i, respectively. The particles are of slightly different size in order to reduce ordering effects. The boundary conditions are based on an experimental realization [13–15]. For more details on other simulations, see [3, 15–18].

In the steady state shear situation where averages are taken, the outer wall is fixed and the inner wall rotates and thus introduces a slow shear deformation in the system. The simulations are started in a dilute state with an extended outer ring while the inner ring already rotates counter-clockwise with constant angular frequency $\Omega = 2\pi/T_i = 0.1\,\mathrm{s}^{-1}$ and period $T_i = 62.83\,\mathrm{s}$. The radius of the outer ring is reduced within about two seconds to reach its desired value R_o and thereafter it is kept fixed. If not explicitly mentioned, averages are performed after about three rotations at $t = 180\,\mathrm{s}$ (to get rid of the arbitrary initial configuration), and during about one rotation, until $t = 239\,\mathrm{s}$.

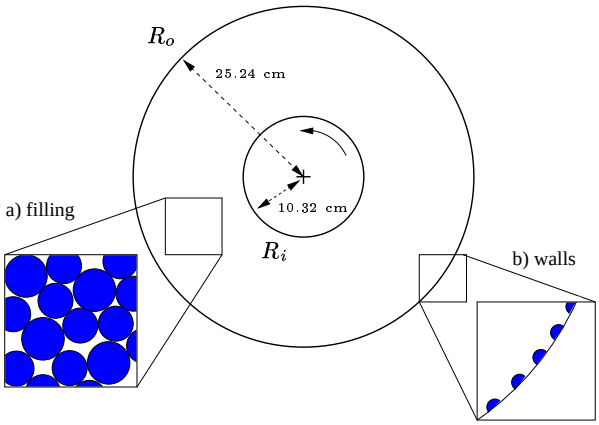

Fig. 1.1. A schematic plot of the model system

In the simulations different global volume fractions $\bar{\nu} = \frac{1}{V_{\mathrm{tot}}} \sum_{p=1}^{N} V^p$ of the shear-cell are examined. The sum runs over all particles p with height h, diameter d_p and thus volume $V^p = \pi h (d_p/2)^2$ in the cell with $V_{\mathrm{tot}} = \pi h (R_o^2 - R_i^2)$. In this study three different $\bar{\nu}$ are examined. In the following the simulations will be referred to as A, B and C with $\bar{\nu} = 0.8084$, 0.8149 and 0.8194, respectively. For the different simulations the number of large and small particles is varied like N_{small}: 2511, 2545, 2555 and N_{large}: 400, 394, 399. For the calculation of the global volume fraction, the small particles glued to the wall are counted with half their volume only, and thus contribute with $\bar{\nu}_{\mathrm{wall}} = 0.0047$ to $\bar{\nu}$ [3]. The

Table 1.1. Microscopic material parameters of the model

property	values
diameter d_{small}, mass m_{small}	7.42 mm, 0.275 g
diameter d_{large}, mass m_{large}	8.99 mm, 0.490 g
reference diameter $\tilde{d}$	8.00 mm
wall-particle diameter d_{wall},	2.50 mm
system/disk-height h	6 mm
normal spring constant k_n	352.1 N/m
normal viscous coefficient γ_n	0.19 kg/s
Coulomb friction coefficient μ	0.44
tangential spring constant k_t	267.1 N/m
bottom friction coefficient μ_b	2×10^{-5}
material density ϱ_0	1060 $\mathrm{kg\,m^{-3}}$

properties of the particles, i.e. the parameters used for the force laws described in detail in the next subsection, are summarized in table 1.1.

1.2.2 The Discrete Element Model

The elementary units of granular materials are mesoscopic grains. In our simulations [3] the grains are treated as rigid particles but deform locally at their contact points. We relate the interaction forces to the virtual overlap δ and to the tangential displacement of two particles during contact. The force laws used are material dependent and have to be validated by comparison with experimental measurements [19–21].

When the force $\boldsymbol{f}_i$ acting on particle i is known (contributions to $\boldsymbol{f}_i$ stem either from other particles, from boundaries or from external forces), the problem is reduced to the integration of Newton's equations of motion. Since we are performing two dimensional (2D) simulations, we have three equations for each particle, two for the linear and one for the rotational degree of freedom [3]. Particle-particle interactions are short range and active on contact only; attractive forces and the presence of other phases are neglected, i.e. we focus on "dry granular media". In the following the force laws accounting for excluded volume, dissipation, and friction are introduced.

Two particles i and j, with diameter d_i and d_j, respectively, interact only when they are in contact so that their overlap $\delta = \frac{1}{2}(d_i + d_j) - (\boldsymbol{r}_i - \boldsymbol{r}_j) \cdot \boldsymbol{n}$ is positive, with the position vector $\boldsymbol{r}_i$ of particle i and the unit vector $\boldsymbol{n} = (\boldsymbol{r}_i - \boldsymbol{r}_j)/|\boldsymbol{r}_i - \boldsymbol{r}_j|$ that points from j to i. The symbol '$\cdot$' denotes the scalar product of vectors. The force $\boldsymbol{f}_i^c$ acting on particle i at its contact c with particle j is decomposed as $\boldsymbol{f}_i^c = \boldsymbol{f}_{\mathrm{n,el}} + \boldsymbol{f}_{\mathrm{n,diss}} + \boldsymbol{f}_{\mathrm{t}}$. The first contribution to the force – accounting for the excluded volume of each particle – is an repulsive elastic force

$$\boldsymbol{f}_{\mathrm{n,el}} = k_n \delta \boldsymbol{n} \ , \tag{1.1}$$

where k_n is proportional to the material's modulus of elasticity. Since we are interested in disks rather than spheres, we use a linear spring that follows Hooke's law, whereas in the case of elastic spheres, the Hertz contact law would be more appropriate.

The second contribution, a viscous dissipation, is given by the damping force in the normal direction

$$\boldsymbol{f}_{\mathrm{n,diss}} = \gamma_n \dot{\delta} \boldsymbol{n} \ , \tag{1.2}$$

where γ_n is a phenomenological, viscous dissipation coefficient and $\dot{\delta} = -\boldsymbol{v}_{ij} \cdot \boldsymbol{n} = -(\boldsymbol{v}_i - \boldsymbol{v}_j) \cdot \boldsymbol{n}$ is the relative velocity in the normal direction. The two normal components are simply added to $\boldsymbol{f}_{\mathrm{n}} = \boldsymbol{f}_{\mathrm{n,el}} + \boldsymbol{f}_{\mathrm{n,diss}}$.

The third contribution to the contact force – accounting for tangential friction – can be chosen in the simplest case, according to Coulomb, as $\boldsymbol{f}_{\mathrm{t,c}} \leq -\mu |\boldsymbol{f}_{\mathrm{n}}| \boldsymbol{t}$, where μ is the friction coefficient and $\boldsymbol{t} = \boldsymbol{v}_{ij}^t / |\boldsymbol{v}_{ij}^t|$ is the tangential unit-vector parallel to the tangential component of the relative velocity $\boldsymbol{v}_{ij}^t = \boldsymbol{v}_{ij} - (\boldsymbol{v}_{ij} \cdot \boldsymbol{n})\boldsymbol{n}$. Since $\boldsymbol{f}_{\mathrm{t,c}}$ is non-smooth and undetermined at $\boldsymbol{v}_{ij}^t = 0$, we also introduced a tangential spring as a necessary ingredient to obtain a positive tangential restitution found from collision experiments with various materials [19]. When two particles get into contact at time t_0, one assumes a "virtual" spring between their contact points, where

$$\eta = \left(\int_{t_0}^{t} \boldsymbol{v}_{ij}^t(t') \mathrm{d}t' \right) \cdot \boldsymbol{t} \tag{1.3}$$

is the total tangential displacement of this spring at time t, build up during contact duration $t - t_0$. Note that due to its definition η can either be positive or negative so that $\boldsymbol{\eta} = \eta \boldsymbol{t}$ can be anti-parallel to $\boldsymbol{t}$. The restoring (static) frictional force, $\boldsymbol{f}_{\mathrm{t,s}} = -k_t \boldsymbol{\eta}$, with the stiffness of the tangential spring k_t, can thus be oriented parallel or anti-parallel to $\boldsymbol{t}$.

The two forces $\boldsymbol{f}_{\mathrm{t,s}}$ and $\boldsymbol{f}_{\mathrm{t,c}}$ are combined by taking the minimum value

$$\boldsymbol{f}_{\mathrm{t}} = -\min(k_t \eta, \mu |\boldsymbol{f}_{\mathrm{n}}|) \boldsymbol{t} \ . \tag{1.4}$$

All contact force components and a bottom friction $\boldsymbol{f}_{\mathrm{b}} = -\mu_b m g \boldsymbol{v}_i / |\boldsymbol{v}_i|$ sum up to the total force

$$\boldsymbol{f}_i = \sum_c (\boldsymbol{f}_{\mathrm{n,el}} + \boldsymbol{f}_{\mathrm{n,diss}} + \boldsymbol{f}_{\mathrm{t}}) + \boldsymbol{f}_{\mathrm{b}} \ . \tag{1.5}$$

1.3 From the Micro- to a Macro-Description

In the previous section, the model system was introduced from the microscopic point of view. In this framework, the knowledge of the forces acting on each particle is sufficient to model the dynamics and the statics of the system. Tensorial quantities like the stress or the deformation gradient are not necessary for a discrete modelling. However, subject of current research is to establish a correspondence to continuum theories by computing tensorial quantities like the

stress $\boldsymbol{\sigma}$, the strain $\boldsymbol{\varepsilon}$, as well as scalar material properties like, e.g., the bulk and shear moduli [6, 8, 9] (see also the chapters of Cambou, Goddard, Kruyt, Lanier and Radjai in this book). In the course of this process, we first discuss averaging strategies, before presenting some results.

1.3.1 Averaging Strategy

Most of the measurable quantities in granular materials vary strongly both in time and on short distances. Thus, during the computation of the averages presented later on, we have to average over or to reduce the fluctuations. In order to suppress the fluctuations, we perform averages in both time and space. This is possible due to the chosen boundary condition. The system can run for a long time in a quasi-steady state and, due to the cylindrical symmetry, all points at a certain distance from the origin are equivalent to each other. Therefore, averages are taken over many snapshots in time with time steps Δt and on rings of material at a center-distance r with width Δr so that the averaging volume of one ring is $V_r = 2\pi h r \Delta r$. For the sake of simplicity (and since the procedure is not restricted to cylindrical symmetry), the averaging volume is denoted by $V = V_r$ in the following. The averaging over many snapshots is somehow equivalent to an ensemble average. However, we remark that different snapshots are not necessarily independent of each other as discussed in [3] and the duration of the simulation might be too short to explore a representative part of the phase space.

Finally, we should remark that the most drastic assumption used for our averaging procedure is the fact, that all quantities are smeared out over one particle. Since it is not our goal to solve for the stress field inside one particle, we assume that a measured quantity is constant inside the particle. This is almost true for the density, but not, e.g., for the stress. However, since we average over all positions with similar distance from the origin, i.e. averages are performed over particles with different positions relative to a ring, details of the position dependency inside the particles will be smeared out anyway.

1.3.2 Averaging Formalism

The mean value of some quantity Q is defined as

$$Q = \frac{1}{V} \sum_{p \in V} w_V^p V^p Q^p \tag{1.6}$$

with the particle volume V^p, the particle quantity $Q^p = \sum_{c=1}^{\mathcal{C}^p} Q^c$, and the quantity Q^c attributed to contact c of particle p which has $\mathcal{C}^p$ contacts. The weight w_V^p accounts for the particle's contribution to the average, and corresponds to the fraction of the particle volume that is covered by the averaging volume. Since an exact calculation of the area of a circular particle that lies in an arbitrary ring is rather complicated, we assume that the boundaries of V are locally straight, i.e. we cut the particle in slices, see [3] for details.

1.4 Results on Macroscopic Scalar Quantities

In the following we apply the averaging formalism to obtain various macroscopic quantities. In table 1.2 the computed quantities as well as the pre-averaged particle quantities are shown. In this study $\otimes$ denotes the dyadic product and '$\cdot$' is used for the order-reduction by one for each of the two tensors at left and right. In the data plots, a rescaled, dimensionless radius $\tilde{r} = (r - R_i)/\tilde{d}$ is used, which gives the distance from the inner wall in units of typical diameters.

Table 1.2. Quantities computed by using the averaging formalism see [3, 17, 18] for details and a derivation

quantity	Q^p	Q
volume fraction ν	1	$\frac{1}{V}\sum_{p\in V} w_V^p V^p$
mass flux density $\nu\boldsymbol{v}$	$\boldsymbol{v}^p$	$\frac{1}{V}\sum_{p\in V} w_V^p V^p \boldsymbol{v}^p$
fabric tensor $\mathbf{F}$ (contact number density)	$\sum_{c=1}^{\mathcal{C}^p} \boldsymbol{n}^c \otimes \boldsymbol{n}^c$	$\frac{1}{V}\sum_{p\in V} w_V^p V^p \sum_{c=1}^{\mathcal{C}^p} \boldsymbol{n}^c \otimes \boldsymbol{n}^c$
stress tensor $\boldsymbol{\sigma}$	$\frac{1}{V^p}\sum_{c=1}^{\mathcal{C}^p} \boldsymbol{f}^c \otimes \boldsymbol{l}^{pc}$	$\frac{1}{V}\sum_{p\in V} w_V^p \sum_{c=1}^{\mathcal{C}^p} \boldsymbol{f}^c \otimes \boldsymbol{l}^{pc}$
deformation gradient $\boldsymbol{\epsilon}$	$\frac{\pi h}{V^p}\sum_{c=1}^{\mathcal{C}^p} \boldsymbol{\Delta}^{pc} \otimes \boldsymbol{l}^{pc} \cdot \mathbf{A}$	$\frac{\pi h}{V}\left(\sum_{p\in V} w_V^p \sum_{c=1}^{\mathcal{C}^p} \boldsymbol{\Delta}^{pc} \otimes \boldsymbol{l}^{pc}\right) \cdot \mathbf{A}$ with $\mathbf{A} = \mathbf{F}^{-1}$

1.4.1 Volume Fraction

As a first example for an averaged scalar quantity, the local volume fraction ν, see Tab. 1.2, is computed. The volume fraction (related to the local density $\varrho(r) \approx \varrho^p \nu$ with the material density ϱ^p) is shown in Fig. 1.2 rescaled in units of ΩR_i. Starting from a nearly uniform volume fraction over the whole cell, after three rotations, a dilated zone forms near to the inner wheel as a consequence of the applied shear. This effect is less pronounced for higher initial global densities. In the outer region of the shear cell ($\tilde{r} > 10$), the structure of the packing remains frozen, i.e. not much reorganization takes place within the duration of the simulation.

1.4.2 Mass Flux Density

As a second scalar quantity, the tangential component of the mass flux density νv_ϕ is investigated. Dividing the mass flux density by the volume fraction, one

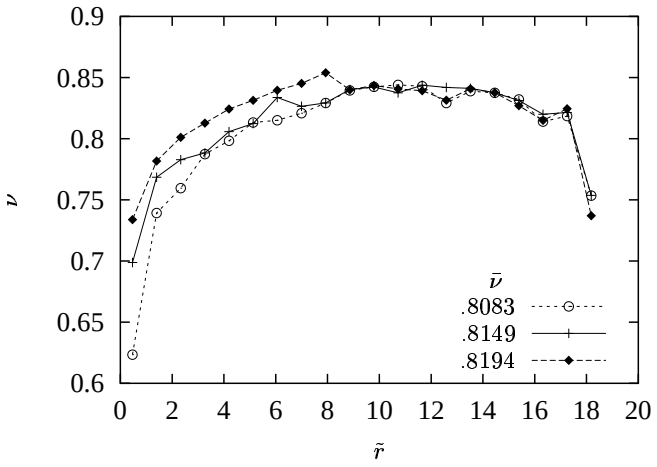

Fig. 1.2. Volume fraction ν, plotted against the dimensionless distance from the origin $\tilde{r}$, for different initial global densities $\bar{\nu}$

gets the tangential velocity v_ϕ shown in Fig. 1.3. The simulation data are fitted by $v_\phi(r) = v_0 \exp(-\tilde{r}/s)$ with v_o: 0.670, 0.756, 0.788 and s: 1.662, 1.584, 1.191, thus showing an exponential profile corresponding to the shear band (forced close to the inner ring by our boundary conditions). The shear band, has a width of a few (~ 8) particle diameters, before the velocity v_ϕ reaches the noise level.

Given the velocity field, it is possible to compute the velocity gradient $\boldsymbol{\nabla v}$ by means of numerical differentiation. From $\boldsymbol{\nabla v}$ one can derive the deformation rate $D_{r\phi} = \frac{1}{2}\left[\frac{\partial v_\phi}{\partial r} - \frac{v_\phi}{r}\right]$ and the continuum rotation rate $W_{r\phi} = \frac{1}{2}\left[\frac{\partial v_\phi}{\partial r} + \frac{v_\phi}{r}\right]$, see [17] for details and [22] for a similar approach.

1.5 Macroscopic tensorial quantities

In this section, the averaged, macroscopic tensorial quantities in our model system are presented. The fabric tensor describes the contact network, the stress tensor describes the stress distribution due to the contact forces, and the elastic deformation gradient is a measure for the corresponding elastic, reversible deformations.

1.5.1 Fabric Tensor

In assemblies of grains, the forces are transmitted from one particle to the next only at the contacts of the particles. Therefore the local geometry and direction of each contact is important [3, 23]. The fabric tensor in table 1.2 is

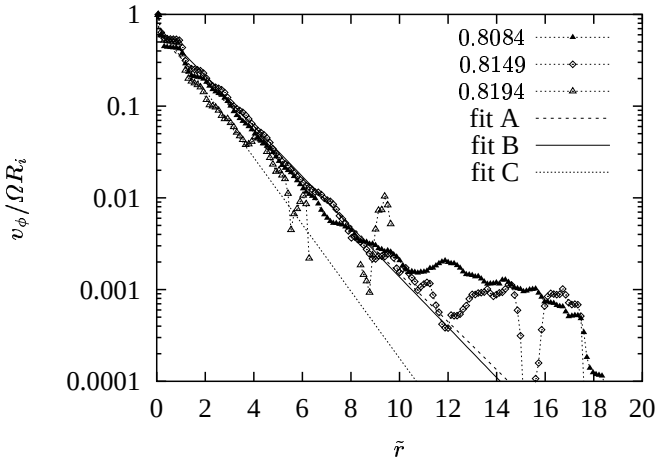

Fig. 1.3. Tangential velocity v_ϕ normalized by the velocity of the inner wheel ΩR_i, plotted against $\tilde{r}$. The lines are the fits to the simulation data for $\tilde{r} = 0.25\text{to}8.1$, using $v_\phi(r) = v_0 \exp(-\tilde{r}/s)$ with v_o: 0.670, 0.756, 0.788 and s: 1.662, 1.584, 1.191, for increasing density, as given in the inset, respectively

symmetric by definition and thus consists of up to three independent scalar quantities in two dimensions. The first of them, the trace (or volumetric part) $F_V = \mathrm{tr}(\mathbf{F}) = (F_{\max} + F_{\min})$, is the contact number density, with the major and the minor eigenvalues $F_{\max}$ and $F_{\min}$, respectively. With other words, one obtains the relation $\mathrm{tr}(\mathbf{F}) = \nu\mathcal{C}$ with reasonable accuracy, where $\mathcal{C}$ is the average number of contacts per particle.

The second scalar, the deviator $F_D = F_{\max} - F_{\min}$, accounts for the anisotropy of the contact network to first order, and the third, the angle ϕ_F, gives the orientation of the "major eigenvector", i.e. the eigenvector corresponding to $F_{\max}$, with respect to the radial outwards direction. In other words, the contact probability distribution is proportional to the function $F_V + F_D \cos(2(\phi - \phi_F))$ [3,16], when averaged over many particles, an approximation which is not always reasonable [24].

The trace of the fabric tensor and the mean number of contacts increases with increasing distance from the inner ring, and is reduced in the vicinity of the walls due to ordering. With increasing local density, the trace of $\mathbf{F}$ is systematically increasing, while the deviatoric fraction F_D/F_V seems to decrease; this means that a denser system is more isotropic concerning the fabric. The major eigendirection is tilted counter-clockwise (for counter-clockwise rotation of the inner ring) by somewhat more than $\pi/4$ from the radial outwards direction, except for the innermost layer and for the strongly fluctuating outer region, where the small deviator does not allow for a proper definition of ϕ_F anyway.

1.5.2 Stress Tensor

The stress tensor, see table 1.2, is proportional to the dyadic product of the force $\boldsymbol{f}^c$ acting at a contact c with its branch vector $\boldsymbol{l}^{pc}$, which accounts for the distance over which the force is transmitted, see [3] for details. The trace of the stress tensor, i.e. the volumetric stress, is almost constant over the whole shear-cell besides fluctuations. In contrast, the non-diagonal elements of $\boldsymbol{\sigma}$ decay proportional to r^{-2} with increasing distance r from the inner ring. The deviatoric fraction σ_D/σ_V also decays like F_D/F_V, when moving outwards from the shear band at the inner ring.

1.5.3 Elastic Deformation Gradient

To achieve the material properties of a granular ensemble one is interested in the stress-strain relationship of the material. The strain $\boldsymbol{\varepsilon}$ can be obtained by time integration of the velocity gradient, see subsection 1.4.2, and subsequent symmetrization and linearization. We present an alternative technique, the application of "Voigt's hypothesis" which assumes that the deformation is uniform and that every particle displacement conforms to the corresponding mean displacement field, but fluctuates about [3, 25].

This relates the actual deformations to a "virtual" reference state where all contacts start to form, i.e. particles are just touching with $\delta = 0$, see [3] for a detailed derivation. The result is a non-symmetric tensor $\boldsymbol{\epsilon}$, which is *not* the strain, instead we refer to it as the elastic deformation gradient, see table 1.2.

The volumetric part of the elastic deformation gradient is largest in the shear zone and this effect is stronger the lower the global density. It is easier to compress the dilute material closer to the inner ring, as compared to the denser material in the outer part. The deviatoric fraction of $\boldsymbol{\epsilon}$, is also decaying with increasing distance from the center, similar to the deviatoric fractions of fabric and stress.

1.5.4 Material Properties

At first we have a closer look on the orientations of the tensors plotted in Fig. 1.4 in the inner part of the shear cell. In the outer part, the deviatoric fraction is usually around 10 per-cent, i.e. so small that the orientations become too noisy to allow for a proper definition. We find that all orientation angles ϕ show the same qualitative behavior, however, the fabric is tilted more than the stress which, in turn, is tilted more than the deformation gradient. Thus, the three tensorial quantities examined so far are *not* co-linear.

We also compute the mean-field expectation values for $\boldsymbol{\sigma}$ and $\boldsymbol{\epsilon}$, in order to get a rough estimate for the orders of magnitude of the following results. Replacing $\boldsymbol{f}^c$ by its mean $\bar{\boldsymbol{f}} = k_n \bar{\delta} \boldsymbol{n}^c$, the radius a_p by $a = \bar{a}$, $\boldsymbol{l}^{pc}$ by $a\boldsymbol{n}^c$, and k_n/h by k_n' one gets $\bar{\boldsymbol{\sigma}} = (k_n' \bar{\delta}/\pi a)\, \mathbf{F}$ for the stress. Performing some similar replacements for the elastic deformation gradient leads to $\bar{\boldsymbol{\epsilon}} = (\pi/k_n')\, \bar{\boldsymbol{\sigma}} \cdot \mathbf{A} = (\bar{\delta}/a)\, \mathbf{I}$.

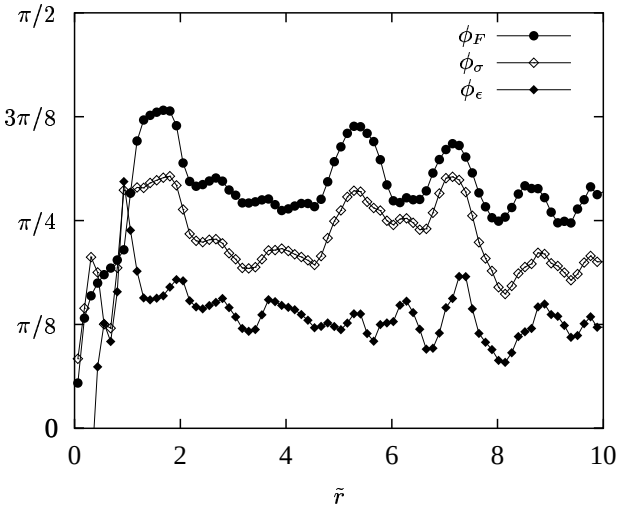

Fig. 1.4. Orientation of the tensors $\mathbf{F}$, $\boldsymbol{\sigma}$, and $\boldsymbol{\epsilon}$, plotted against the distance from the inner ring from simulation B. The data are shown only for about 10 layers of particles counted from the inner ring. Solid circles are fabric, open diamonds are stress, and solid diamonds are elastic deformation gradient data

The material stiffness, $\bar{E}$, can be defined as the ratio of the volumetric parts of stress and strain, so that one obtains the mean field prediction

$$\bar{E} = (k_n'/2\pi)\,\mathrm{tr}(\mathbf{F}) \ . \tag{1.7}$$

In Fig. 1.5 the rescaled stiffness of the granulate is plotted against the trace of the fabric for all simulations. Note that all data collapse almost on a line, but the mean-field value underestimates the simulation data by some per-cent. Additional simulation data (not shown here) for different k_n and even data from simulations with neither bottom- nor tangential friction collapse with the data for fixed k_n and different volume fractions, shown here. The few data points which deviate most are close to the boundaries, where the material is strongly layered. The deviation from the mean field prediction (*solid* line in Fig. 1.5) seems to disappear in the absence of shear – a fact which can be accepted since the mean field expression (1.7) does not account for the shear displacement.

In Fig. 1.6 the ratio of the deviatoric parts of stress and strain is plotted against the trace of the fabric. We did not use the traditional definition of the shear modulus [8], since our tensors are not co-linear as shown in Fig. 1.4. Like the material stiffness, both quantities are proportional, for points near or within the shear band. In the outer part of the shear-cell the particles are strongly inter-locked and thus resist much more against shear, and therefore G diverges. For increasing global density, the critical contact number density also grows, at a critical density.

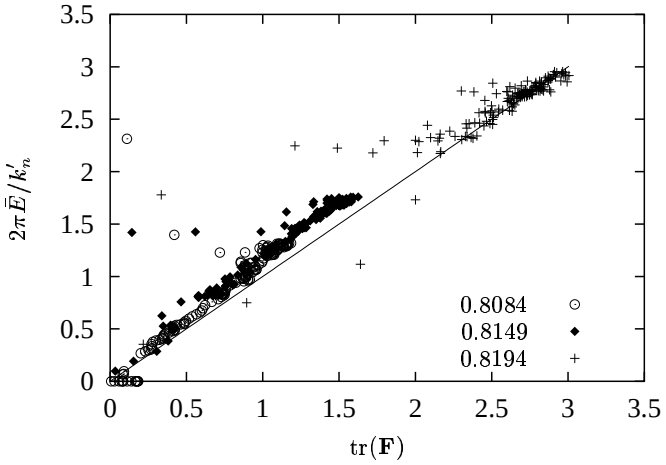

Fig. 1.5. Granulate stiffness $2\pi\bar{E}/k_n' = \mathrm{tr}(\boldsymbol{\sigma})/\mathrm{tr}(\boldsymbol{\epsilon})$, plotted against $\mathrm{tr}(\mathbf{F})$ from all simulations. Every point corresponds to one ring of 150, i.e. $\Delta r \approx (1/8)d_{\mathrm{small}}$

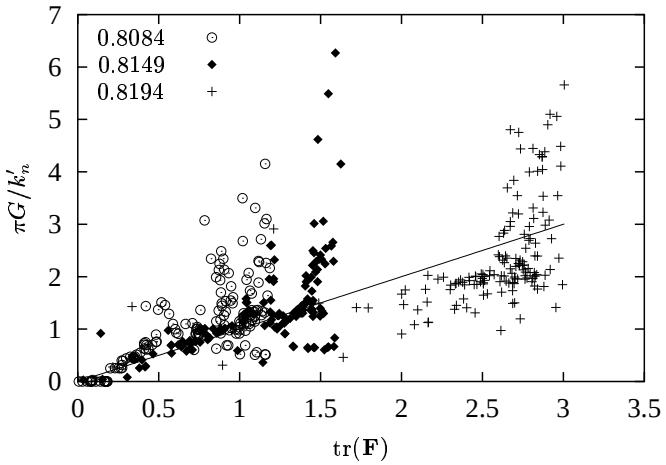

Fig. 1.6. Scaled granulate shear resistance $\pi G/k_n' = \mathrm{dev}(\boldsymbol{\sigma})/\mathrm{dev}(\boldsymbol{\epsilon})$ plotted against $\mathrm{tr}(\mathbf{F})$ from all simulations. The line indicates the identity curve

1.6 Rotational Degrees of Freedom

The particles in the model are able to rotate so that also quantities concerning the rotational degree of freedom are of interest [22]. In Fig. 1.7 the macroscopic

particle rotations ω, the continuum rotation $W_{r\phi}$ and the excess rotation $\omega^* = \omega - W_{r\phi}$, are displayed. The spin is averaged using $Q^p = \omega^p$ in Eq. (1.6) so that one obtains the spin density

$$\nu\omega = \frac{1}{V} \sum_{p \in V} w_V^p V^p \omega^p \ , \tag{1.8}$$

in analogy to the mass flux density.

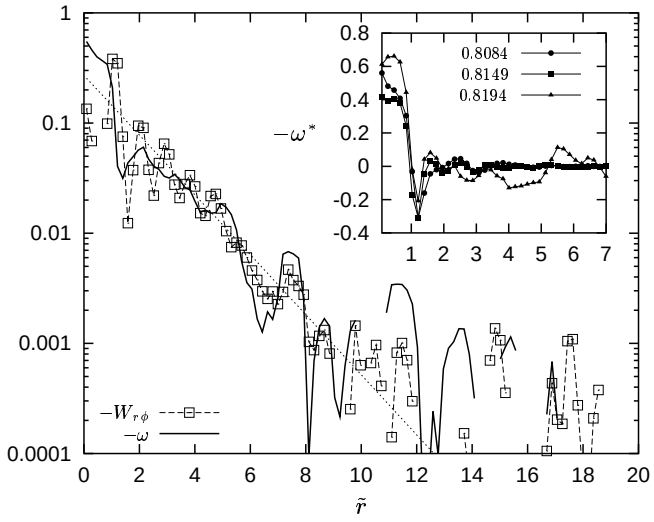

Fig. 1.7. Angular velocities ω (*solid line*) and $W_{r\phi}$ (*symbols*) of the particles and the continuum, plotted against the scaled radial distance (from simulation B). The *dotted* line is $W_{r\phi}$ as obtained from the fit to v_ϕ, see subsection 1.4.2. In the inset, the excess spin is displayed for all simulations

As it can be seen in Fig. 1.7, both the particle and the continuum rotation decay exponentially with increasing $\tilde{r}$, similar to the velocity v_ϕ. The inset of Fig. 1.7 shows an oscillation of the excess rotation near the inner wheel, from one disk layer to the next. This is due to the fact that the disks in adjacent layers are able roll over each other in the shear zone.

Because of the evident importance of the rotational degree of freedom, this we use the theoretical framework of a Cosserat continuum [22, 26, 27]. In addition to the stress and the displacement gradient one can define the couple stress $\mathbf{M}$ and the curvature $\boldsymbol{\kappa}$. The couple stress tensor is defined here, in analogy to the stress, as

$$\mathbf{M} = \frac{1}{V} \sum_{p \in V} w_V^p \sum_{c=1}^{\mathcal{C}^p} (\boldsymbol{l}^{pc} \times \boldsymbol{f}^c) \otimes \boldsymbol{l}^{pc} \ , \tag{1.9}$$

where the force is replaced by the torque due to the tangential component of the force, and the '$\times$' denotes the vector-product. In a two dimensional system, only the two components M_{zr} and $M_{z\phi}$ of the tensor are non-zero. The values of M_{zr} as a function of $\tilde{r}$ are shown in Fig. 1.8(a). Note that $\mathbf{M} = \mathbf{0}$, when the sum of the torques acting on one particle vanishes in static equilibrium. In our steady state shear situation $\mathbf{M}$ fluctuates around zero, except for a large value in the shear band, close to the inner wall. In analogy to $\boldsymbol{\epsilon}$ we define

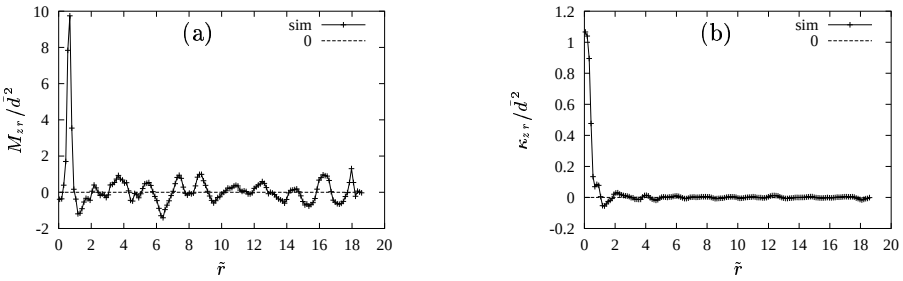

Fig. 1.8. (**a**) Plot of the couple stress $M_{zr}/\tilde{d}^2$ against $\tilde{r}$, (**b**) plot of the curvature $\kappa_{zr}/\tilde{d}^2$ against $\tilde{r}$ from simulation B

$$\boldsymbol{\kappa} = \frac{\pi h}{V}\left(\sum_{p\in V} w_V^p \sum_{c=1}^{C^p} (\boldsymbol{l}^{pc} \times \boldsymbol{\Delta}^{pc}) \otimes \boldsymbol{l}^{pc}\right) \cdot \boldsymbol{A} \ , \tag{1.10}$$

where the local contact displacement $\boldsymbol{\Delta}^{pc}$ is replaced by the corresponding angular vector $\boldsymbol{l}^{pc} \times \boldsymbol{\Delta}^{pc}$. The values of the curvature κ_{zr} are plotted in Fig. 1.8(b) against $\tilde{r}$ with similar qualitative behavior as M_{zr}. The other components $M_{z\phi}$ and $\kappa_{z\phi}$ lead to no new insights and are omitted here.

Since we are interested in the role the rotational degree of freedom plays for the constitutive equations, we define the "torque resistance" μ_c as the ratio of the magnitudes of the couple stress and the curvature components. This quantity describes how strongly the material resists against applied torques. In Fig. 1.9 the torque resistance is plotted for the three simulations. In the dilute regions near the inner wheel, where the particles are able to rotate more easily, μ_c is smaller than in the dense outer part, where the particles are interlocked and thus frustrated. This behavior is consistent with the results for increasing global densities, i.e. the torque resistance increases with density. Note that the strongest fluctuations are due to the division by small κ_{zr} values and have no physical meaning in our interpretation.

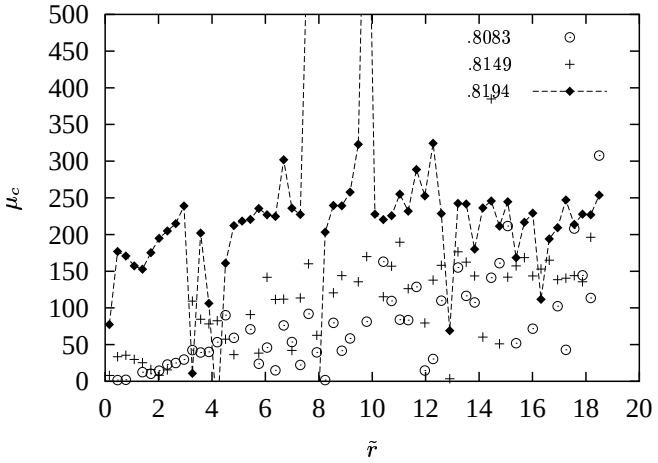

Fig. 1.9. Torque resistance $\mu_c = M_{zr}/\kappa_{zr}$ plotted against $\tilde{r}$ for all simulations.

1.7 Summary and Conclusion

Discrete element simulations of a 2D Couette shear cell were presented and used as the basis for a micro-macro averaging procedure. The boundary conditions were chosen to allow for averaging over large volumes (rings with width Δr, where Δr can be much *smaller* than the particle diameter) and over a steady state shear and thus over long times. A shear band is localized close to the inner, rotating cylindrical wall. The configurations changed rather rapidly in the shear band, whereas the system is almost frozen in the outer part.

The averaging strategy used assumes the quantities to be homogeneously smeared out over the whole particle which is cut in slices by the averaging volumes. This so called slicing method shows discretization effects in the range of averaging volume widths Δr from about one to one fifth of a particle diameter, whereas the results become independent of the size of the averaging volume for smaller Δr. For Δr much larger than the particle-size, the microscopic details – including rotations – are not longer resolved properly.

The material density, i.e. the volume fraction, the coordination number, the fabric tensor, the stress tensor and the elastic, reversible deformation gradient were obtained by the averaging procedure. The fabric is linearly proportional to the product of volume fraction and coordination number. In the shear band, dilation together with a reduction of the number of contacts is observed. The mean volumetric stress is constant in radial direction while the mean deformation gradient decays with the distance from the inner wall. The ratio of the volumetric parts of stress and strain gives the material stiffness of the granulate, which is small in the shear band and larger outside, due to dilation.

In the shear band, large deviators, i.e. anisotropy, of all tensorial quantities are found, however, decreasing algebraically with increasing distance from the inner wall. The isotropy of the tensors grows only slightly with increasing density and all tensors are tilted counter-clockwise from the radial direction by an angle of the order of $\pi/4$. The system organizes itself such that more contacts are created to act against the shear and also the shear resistance increases with the contact density. An essential result is that the macroscopic tensors are *not* co-linear, i.e. their orientations are different. The orientation of the fabric is tilted most, that of the deformation gradient is tilted least and thus, the material cannot be described by a simple elastic model involving only the two Lamé constants (or bulk modulus and Poisson's ratio) as the only parameters. The stress and the deformation gradient are seemingly interconnected via the fabric tensor.

Finally, the particle rotation was measured in analogy to the particle velocity. Subtraction of the continuum rotation from the particle rotation leads to the excess eigen-rotation of the particles with respect to the mean rotation, in the spirit of a micro-polar or Cosserat continuum theory. In analogy to the stress and elastic deformation gradient, we defined couple stress and curvature. The quotient of the respective non-zero components gives a "torque-resistance" which increases with increasing local density and stress.

References

1. H. J. Herrmann, J.-P. Hovi, and S. Luding, editors. *Physics of dry granular media - NATO ASI Series E 350.* Kluwer Academic Publishers, Dordrecht, 1998.
2. P. A. Cundall and O. D. L. Strack. A discrete numerical model for granular assemblies. *Géotechnique*, 29(1):47–65, 1979.
3. M. Lätzel, S. Luding, and H. J. Herrmann. Macroscopic material properties from quasi-static, microscopic simulations of a two-dimensional shear-cell. *Granular Matter*, 2(3):123–135, 2000. cond-mat/0003180.
4. L. Rothenburg and A. P. S. Selvadurai. A micromechanical definition of the cauchy stress tensor for particulate media. In A. P. S. Selvadurai, editor, *Mechanics of Structured Media*, pages 469–486. Elsevier, 1981.
5. P. A. Cundall, A. Drescher, and O. D. L. Strack. Numerical experiments on granular assemblies; measurements and observations. In *IUTAM Conference on Deformation and Failure of Granular Materials*, pages 355–370, Delft, 1982.
6. J. D. Goddard. Microstructural origins of continuum stress fields - a brief history and some unresolved issues. In D. DeKee and P. N. Kaloni, editors, *Recent Developments in Structered Continua. Pitman Research Notes in Mathematics No. 143*, page 179, New York, 1986. Longman, J. Wiley.
7. R. J. Bathurst and L. Rothenburg. Micromechanical aspects of isotropic granular assemblies with linear contact interactions. *J. Appl. Mech.*, 55:17, 1988.
8. N. P. Kruyt and L. Rothenburg. Micromechanical definition of strain tensor for granular materials. *ASME Journal of Applied Mechanics*, 118:706–711, 1996.
9. C.-L. Liao, T.-P. Chang, D.-H. Young, and C. S. Chang. Stress-strain relationship for granular materials based on the hypothesis of best fit. *Int. J. Solids Structures*, 34:4087–4100, 1997.

10. E. Kuhl, G. A. D´Addetta, H. J. Herrmann, and E. Ramm. A comparison of discrete granular material models with continuous microplane formulations. *Granular Matter*, 2:113–121, 2000.
11. F. Dedecker, M. Chaze, Ph. Dubujet, and B. Cambou. Specific features of strain in granular materials. *Mech. Coh. Fric. Mat.*, 5:174–193, 2000.
12. F. Calvetti, G. Combe, and J. Lanier. Experimental micromechanical analysis of a 2d granular material: relation between structure evolution and loading path. *Mech. Coh. Fric. Mat.*, 2:121–163, 1997.
13. D. Howell and R. P. Behringer. Fluctuations in a 2d granular Couette experiment: A critical transition. *Phys. Rev. Lett.*, 82:5241, 1999.
14. C. T. Veje, D. W. Howell, and R. P. Behringer. Kinematics of a 2D granular Couette experiment. *Phys. Rev. E*, 59:739, 1999.
15. C. T. Veje, D. W. Howell, R. P. Behringer, S. Schöllmann, S. Luding, and H. J. Herrmann. Fluctuations and flow for granular shearing. In H. J. Herrmann, J.-P. Hovi, and S. Luding, editors, *Physics of Dry Granular Media*, page 237, Dordrecht, 1998. Kluwer Academic Publishers.
16. S. Schöllmann. Simulation of a two-dimensional shear cell. *Phys. Rev. E*, 59(1):889–899, 1999.
17. S. Luding, M. Lätzel, and H. J. Herrmann. From discrete element simulations towards a continuum description of particulate solids. In H. Kalman, A. Levy, and M. Hubert, editors, *The Third Israeli Conference for Conveying and Handling of Particulate Solids*, pages 3.125–3.130, Tel-Aviv, 2000. The Forum for Bulk Solids Handling.
18. S. Luding, M. Lätzel, W. Volk, S. Diebels, and H. J. Herrmann. From discrete element simulations to a continuum model. In *European Congress on Computational Methods in Applied Sciences and Engineering, ECCOMAS 2000*, Barcelona, 2000. in press.
19. S. F. Foerster, M. Y. Louge, H. Chang, and K. Allia. Measurements of the collision properties of small spheres. *Phys. Fluids*, 6(3):1108–1115, 1994.
20. L. Labous, A. D. Rosato, and R. Dave. Measurements of collision properties of spheres using high-speed video analysis. *Phys. Rev. E*, 56:5715, 1997.
21. E. Falcon, C. Laroche, S. Fauve, and C. Coste. Behavior of one inelastic ball bouncing repeatedly off the ground. *Eur. Phys. J. B*, 3:45–57, 1998.
22. A. Zervos, I. Vardoulakis, M. Jean, and P. Lerat. Numerical investigation of granular interfaces kinematics. *Mech. Cohes.-Frict. Matter*, 5:305–324, 2000.
23. J. D. Goddard. Continuum modeling of granular assemblies. In H. J. Herrmann, J.-P. Hovi, and S. Luding, editors, *Physics of Dry Granular Media*, pages 1–24, Dordrecht, 1998. Kluwer Academic Publishers.
24. M. M. Mehrabadi, S. Nemat-Nasser, H. M. Shodja, and G. Subhash. Some basic theoretical and experimental results on micromechanics of granular flow. In *Micromechanics of granular media*, Amsterdam, 1988. Elsevier.
25. C.-L. Liao and T.-C. Chang. A generalized constitutive relation for a randomly packed particle assembly. *Computers and Geotechnics*, 20(3/4):345–363, 1997.
26. E. Cosserat and F. Cosserat. *Theorie des Corps Deformables.* Herman et fils, Paris, 1909.
27. A. C. Eringen. Theory of micropolar elasticity. In H. Liebowitz, editor, *Fracture*, volume 2, pages 621–729, New York and London, 1968. Academic Press.